Applied Catalysis B: Environmental 138–139 (2013) 26–32

Contents lists available at SciVerse ScienceDirect

Applied Catalysis B: Environmental

journal homepage: www.elsevier.com/locate/apcatb

Production of visible activity and UV performance enhancement of ZnO photocatalyst via vacuum deoxidation

Yanhui Lv, Chengsi Pan, Xinguo Ma, Ruilong Zong, Xiaojuan Bai, Yongfa Zhu*

Department of Chemistry, Tsinghua University, Beijing 100084, PR China

ARTICLE INFO

Article history:
Received 13 December 2012
Received in revised form 21 January 2013
Accepted 3 February 2013
Available online 20 February 2013

Keywords:
Photocatalysis
Vacuum Deoxidation
ZnO
Surface oxygen vacancy

ABSTRACT

ZnO photocatalyst with surface oxygen vacancies was obtained via vacuum deoxidation method. The concentration of surface oxygen vacancies could be controlled by tuning the temperature and time in vacuum, which governs the production of visible activity and the enhanced level of photocatalytic activity. The optimum UV photocatalytic activity and photocurrent of vacuum ZnO are almost 1.7 and 2.4 times as high as that of pure ZnO, respectively. Interestingly, the dramatic visible photocatalytic activity and distinct photocurrent both are generated due to the introducing of oxygen vacancies on ZnO surface. The enhancement in performance is attributed to the high separation efficiency of photogeneration electron–hole pairs due to the broadening of the valance band (VB) induced by surface oxygen-vacancies states. The production of visible photoactivity is demonstrated to be the narrow of energy band gap resulting from the rising of VB.

1. Introduction

In the past decades, extensive research efforts have been devoted to the development of photocatalytic materials for eliminating organic and inorganic pollutants by utilizing natural solar energy [1–6]. ZnO is one of the most widely used photocatalysts due to the advantages of inexpensive, low toxicity and robustness [7–9]. Nevertheless, because of the wide band gap (3.2 eV), ZnO photocatalyst absorbs mainly in the UV region, it is hardly no visible response. Many studies found that visible photocatalytic activity of metal oxide semiconductors can be obtained by doping with metals [10], and nonmetals [11,12], cations [13], anions [14], and combining with another semiconductor [15]. However, most of these methods often need a higher temperature and high pressure or complicated and expensive equipments. More importantly, in the expansion of visible-light response by using these methods, the UV-light activity of ZnO photocatalyst almost no increased simultaneity. Therefore, it is very important to find a new simple method for application of ZnO, not only fabricating visible photocatalytic activity but also improving UV photoactivity.

In this work, an economical and facile method, vacuum deoxidation, is introduced to fabricate oxygen vacancies on ZnO surface. The visible photoactivity is produced and the UV photoactivity is greatly improved via surface oxygen vacancies for ZnO photocatalyst. It is considered that the concentration of surface oxygen vacancies is controlled by tuning the temperature and the time in the process of vacuum treatment. Oxygen vacancies are formed on the surface of ZnO photocatalyst and no changes in crystal structure. The best photocatalytic performances are obtained for ZnO after vacuum treated at 255 °C for 5 h (called as vacuum ZnO). The visible photocatalytic activity and photocurrent is highly generated. And the UV photocatalytic activity and photocurrent is increased to about 1.7 and 2.4 times, respectively. So it is an efficient way to produce the visible response and enhance the photocatalytic activities via surface oxygen vacancies introduced on ZnO by vacuum deoxidation.

2. Experimental

2.1. Materials preparation

ZnO with diameter of 30–50 nm and surface area 10.4 $m^2 g^{-1}$ was commercially available. All other chemicals used were reagent grade without further purification. Vacuum deoxidation treated ZnO samples were prepared as follows: (1) the temperature programmed deoxidizing (TPD) measurement using helium (He) gas was performed in a specially designed quartz tube with 0.030 g of nanometer ZnO sample. The tube was put in a cylindrical electric furnace. Temperature of the furnace was controlled by a programmable regulator with the thermocouple. A thermal conductivity detector (TCD) was used to detect He consumption during the vacuum treatment process. ZnO sample was pretreated by

* Corresponding author. Tel.: +86 10 6278 3586; fax: +86 10 6278 7601.
E-mail address: zhuyf@tsinghua.edu.cn (Y. Zhu).

0926-3373/$ – see front matter © 2013 Elsevier B.V. All rights reserved.
http://dx.doi.org/10.1016/j.apcatb.2013.02.011

nitrogen (N_2) gas from room temperature to 200 °C at a temperature ramping rate of 10 °C min^{-1} for 2 h. Then it cooled naturally to the room temperature in N_2 atmosphere. Afterwards, He gas was introduced into the homemade quartz tube equipped with ZnO sample, and the gas flow rate was 30 mL min^{-1} accompanying with the temperature gradually increased to 550 °C for 5 min. (2) According to the TPD graph, it can be seen that the optimum deoxidation temperature range was 240–260 °C. Vacuum deoxidation process (temperature from 240 to 260 °C at 5 °C intervals, time was 3, 4, 5, 7 and 9 h, respectively) was performed to prepare ZnO samples for the photocatalytic degradation reaction. The purchased ZnO powders were put into a self-made quartz tube and then placed into a furnace connected with a vacuum pump and a program heating device. Pressure in the vacuum deoxidation process was about 1×10^{-3}–10^{-4} Torr and the temperature was increased from room temperature to designed temperature at an increasing rate of 10 °C min^{-1}, and the time was kept for 3, 4, 5, 7 and 9 h, respectively. Finally, the samples were cooled naturally to room temperature.

2.2. Characterization

Ultraviolet–visible diffuse reflectance spectroscopy (UV-DRS) was performed in Hitachi U-3010, $BaSO_4$ was used as reference. A high-resolution transmission electron microscope (HR-TEM, JEM 2010F) operated at an accelerating voltage of 200 kV. The room temperature photoluminescence (PL) spectra of ZnO and vacuum ZnO samples were investigated utilizing the PerkinElmer LS55 spectrophotometer equipped with xenon (Xe) lamp with an excitation wavelength of 277 nm. The in situ electron paramagnetic resonance (EPR) measurement was carried out using an Endor spectrometer (JEOL ES-ED3X) at room temperature. The g factor was obtained by taking the signal of manganese as. The EPR spectrometer was coupled to a computer for data acquisition and instrument control. Magnetic parameters of the radicals detected were obtained from direct measurements of magnetic field and microwave frequency. The photocurrent was measured on an electrochemical system (CHI-660B, China). UV light was obtained from an 11 W germicidal lamp and visible light was obtained from a 500 W Xe lamp (Institute for Electric Light Sources, Beijing) with a 420 nm cut-off filter. A standard three-electrode cell with a working electrode, a platinum wire as counter electrode and a standard calomel electrode (SCE) as reference electrode were used in photoelectric studies. 0.1 M Na_2SO_4 was used as the electrolyte solution. Potentials were given with reference to the SCE. The photoelectric responses of the photocatalysts as light on and off were measured at 0.0 V.

2.3. Photocatalytic evaluation

The photocatalytic activities of the as-prepared samples were evaluated by the decomposition of methylene blue (MB) in solution under UV and visible light. UV light source was obtained by an 11 W UV germicidal lamp ($\lambda = 254$ nm) and the average light intensity was 0.96 mW cm^{-2}. 50 mg photocatalyst was added into prepared 100 mL 1×10^{-5} M MB aqueous solution. Before the light irradiation, the suspensions were firstly ultrasonic dispersed in dark for 10 min, then magnetically stirred for 15 min to reach the absorption–desorption equilibrium. At given time intervals, 3 mL aliquots were sampled and centrifuged to remove the photocatalyst particles. Synchronously, the filtrates of MB solutions at different conditions were analyzed by recording variations of the maximum absorption peak in the UV–vis spectra using a Hitachi U-3010 UV–vis spectrophotometer. In addition, the visible light was provided by a halogen–tungsten lamp (power 175 W, $\lambda_{main} = 550$ nm). The average visible light intensity was 2.5 mW cm^{-2}. The method was similar with the UV-light degradation above mentioned.

3. Results and discussion

3.1. Photoactivity of vacuum ZnO

The UV photocatalytic activities of ZnO and ZnO vacuum treated with various temperature and time on the degradation of methylene blue (MB), a hazardous dye as well as a common model to test the photodegradation capability, were investigated. The degradation process is fitted to pseudo-first-order kinetics, and the values of the rate constant k are shown in Fig. 1A, B, respectively. The UV photocatalytic activities of vacuum-treated ZnO samples are gradually enhanced with the increase of vacuum temperature or time; when the temperature attains to 255 °C, time is for 5 h, vacuum ZnO exhibits the highest photocatalytic activity. The apparent rate constant k is 0.1189 min^{-1} and it is about 1.7 times as high as that of untreated ZnO. Further increasing temperature or prolonging time, however, the degradation rate decreases, but it still remains higher than that of untreated ZnO. The greatly improvement of UV photocatalytic activity results from the high charge separation efficiency, which is caused by the expanded of the VB width due to the generation of surface oxygen-vacancies states. The concentration of oxygen vacancies influences the photocatalytic activity of ZnO samples. When the concentration is too low, the photocatalytic activity only improves slightly and enhances gradually with the increase of the surface oxygen-vacancies concentration; while the concentration is too high, bulk oxygen vacancies in ZnO lattice easily generate, which are the recombination center of electron–hole pairs and result in the decrease of photocatalytic activity. So the concentration of surface oxygen vacancies controlled by vacuum temperature and time plays an important role in improving the photocatalytic activity.

The UV photocurrent responses of ZnO and vacuum ZnO after deposition on ITO electrodes are provided in Fig. 1C. A fast and stable photocurrent response is observed for each switch-on and switch-off event in both electrodes. Vacuum ZnO electrode shows a noticeable photocurrent, which is about 2.4 times as high as that of ZnO. The improvement of UV photocurrent verifies that the charge separation efficiency improves greatly. This result is in accord with the improvement of photocatalytic activity for ZnO samples.

The visible photocatalytic activities of ZnO untreated and vacuum treated with various temperature and time on the degradation of MB are shown in Fig. 2A, B ($\lambda_{main} = 550$ nm), respectively. Since ZnO could hardly be excited by visible light, ZnO plays almost no role in degrading MB. However, vacuum-treated ZnO possesses visible activity, especially treated at 255 °C for 5 h. The apparent rate constant $k = 0.4664\ h^{-1}$, which is much higher than that of untreated ZnO ($k = 0.0142\ h^{-1}$). The influences of various vacuum temperature and time on visible activities are as same as that on UV activities of ZnO samples.

In addition, the photocurrents of ZnO and vacuum ZnO electrodes, under visible light ($\lambda > 420$ nm), are shown in Fig. 2C. ZnO electrode is almost no photocurrent response, while vacuum ZnO electrode shows an obvious photocurrent (8 times as high as that of pure ZnO). The enhancement of photocurrent indicates that the separation efficiency of photoinduced electron–hole pairs improves, thus the photocatalytic activity is enhanced greatly. To further understand the mineralization property of the as-prepared photocatalyst, the decreases of TOC in the photodegradation of MB by ZnO and vacuum ZnO photocatalysts are determined. The TOC removal percentage is 6% and 70% for ZnO and vacuum ZnO after 6 h photocatalytic reaction on MB, see from Fig. 2D. It can

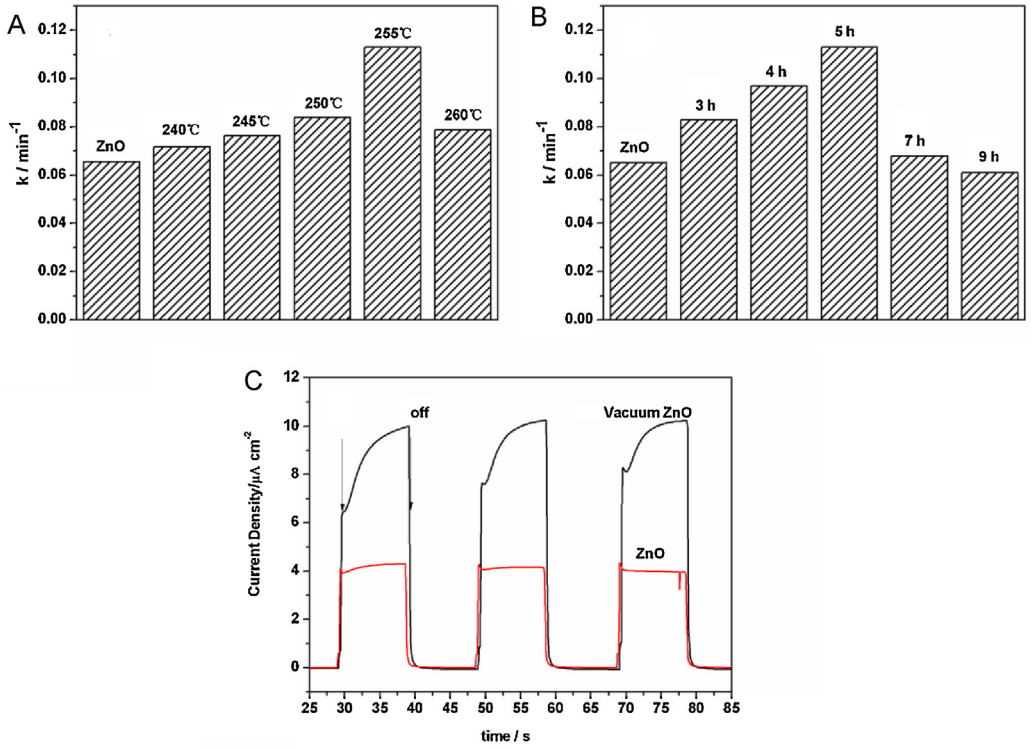

Fig. 1. Comparison of the UV photocatalytic activity of ZnO untreated and vacuum treated with (A) various temperature for 5 h and (B) various time at 255 °C on the degradation of MB, respectively; (C) Photocurrents of ZnO and vacuum ZnO (treated at 255 °C for 5 h) electrodes, under UV light (λ = 254 nm).

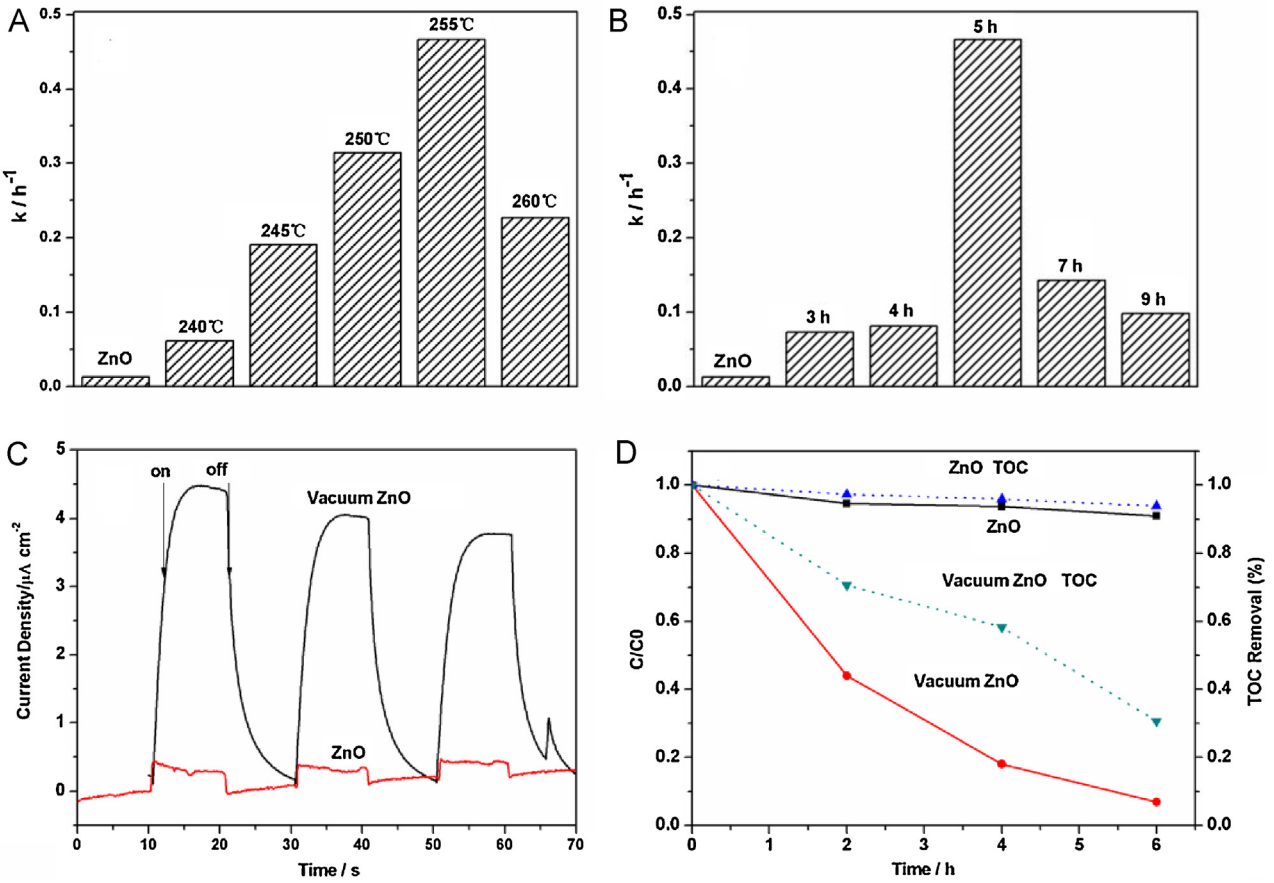

Fig. 2. Comparison of the visible activity of ZnO untreated and vacuum treated with (A) various temperature for 5 h and (B) various time at 255 °C on the degradation of MB (λ_{main} = 550 nm); (C) Photocurrents of ZnO and vacuum ZnO (treated at 255 °C for 5 h) electrodes, (D) TOC removal plots of ZnO and vacuum ZnO (treated at 255 °C for 5 h) on the degradation of MB, under visible light (λ > 420 nm), respectively.

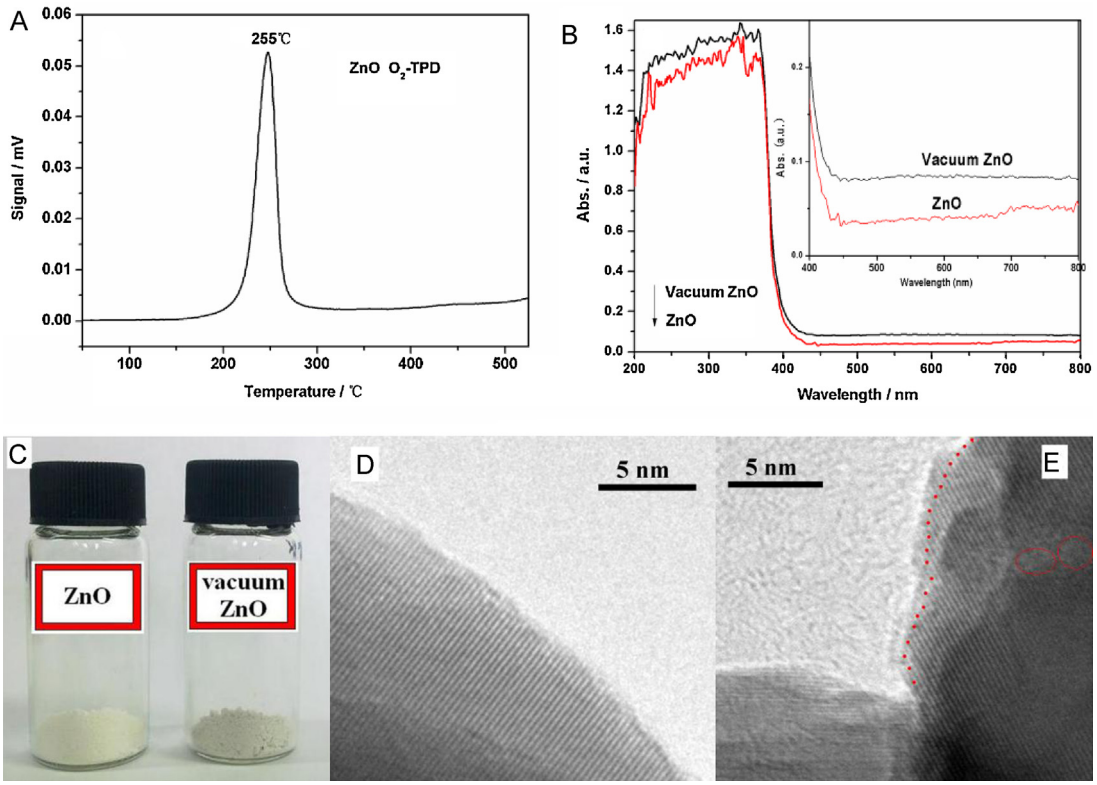

Fig. 3. (A) O_2-TPD profile of ZnO sample; (B) UV–vis diffuse reflectance spectra of ZnO and vacuum ZnO, the inset shows an enlarge from 400 to 800 nm; (C) A photo comparing ZnO and Vacuum ZnO; (D) and (E) HR-TEM images of ZnO and Vacuum ZnO.

be confirmed that the mineralization property of vacuum ZnO is evidently enhanced.

3.2. Formation of surface oxygen vacancy

To investigate the deoxidation process, temperature-programmed deoxidation (TPD) was performed on the ZnO sample, as shown in Fig. 3A. The O_2-TPD profile of ZnO exhibits a narrow and sharp peak at about 255 °C. This peak corresponds to the partial loss of oxygen atoms on ZnO sample, resulting in the formation of oxygen vacancies. From the X-ray diffraction (XRD) patterns of pure ZnO and vacuum ZnO samples Fig. S1, it can be found that no phase transformation or any impurity is observed for ZnO after vacuum deoxidation at 255 °C for 5 h, so there most oxygen atoms are removed from ZnO surface, generating surface oxygen vacancies. UV–vis diffuse reflectance spectra (UV-DRS) of ZnO and vacuum ZnO photocatalysts are shown in Fig. 3**B**. ZnO shows the characteristic spectrum with its fundamental absorption sharp edge at 400 nm. The absorbance edge of vacuum ZnO photocatalysts exhibits only a little redshift, and the inset of Fig. 3B shows that the absorbance of vacuum ZnO parallely enhanced by about 0.05 units in visible-light region (450–800 nm), which maybe induced by surface oxygen vacancies. The color of ZnO samples changes from light yellow to light gray by vacuum deoxidation as shown in Fig. 3C. The untreated ZnO is highly crystallized, as seen from perfect lattice features shown in HR-TEM Fig. 3D. However, the edge of vacuum ZnO particles become disordered (Fig. 3E), which indicates the surface structure is damaged and maybe surface oxygen vacancies is formed. In one word, the concentration of oxygen vacancies, controlled by vacuum temperature and time, influences the sites of oxygen-vacancies states, and the photoresponse range and photocatalytic activity will be affected, accordingly.

To further confirm the existence and properties of oxygen vacancies, electron paramagnetic resonance (EPR) was performed. It can provide a sensitive and direct method to monitor various behaviors to the presence of native defects, such as oxygen vacancies and zinc vacancies [16]. Fig. 4A shows the EPR signal of ZnO and vacuum ZnO. The peak intensity of strong EPR signal at $g \sim 1.957$ of vacuum ZnO is almost as same as that of ZnO, which is represented as neutral shallow donors in single crystals of ZnO [17–24]. However, the EPR signal of vacuum ZnO appears a new peak at $g \sim 2.001$, which can be attributed as surface oxygen vacancies [17,18]. It is reported that the visible photoabsorption can be possibly fabricated by introducing high oxygen vacancy concentration [25–27], due to the narrow of band gap caused by the formation of oxygen-vacancy states.

The photoluminescence (PL) spectra of ZnO and vacuum ZnO were investigated (at wavelength 277 nm excitation), as shown in Fig. 4B. ZnO photocatalyst only shows one wide weak peak, whereas four main emission peaks for vacuum ZnO emerge around 420, 446, 460 and 490 nm, respectively. The emission at ~420 nm (2.95 eV) is attributed to the transition between shallow donors (oxygen vacancy) to the valence band VB [28–30]. A 446 nm (2.78 eV) blue emission peak in ZnO imply that electrons are trapped at interfaces lying within the depletion regions located at ZnO–ZnO grain boundaries [31]. The peak at 460 nm (2.7 eV) is related to Zn vacancy [32]. The 490 nm (2.53 eV) emission is controversial, but the most advantageous argument is the transition should be attributed to the existence of oxygen defects on the surface of photocatalyst [31,33]. It is well known that this visible emission (420–490 nm) is also observed due to transitions of defect states formed by oxygen vacancies [34–36]. Moreover, the larger the concentration of surface oxygen vacancies are, the stronger the PL signal is [37,38]. Therefore, comparing with pure ZnO, more surface oxygen vacancies are produced on vacuum ZnO.

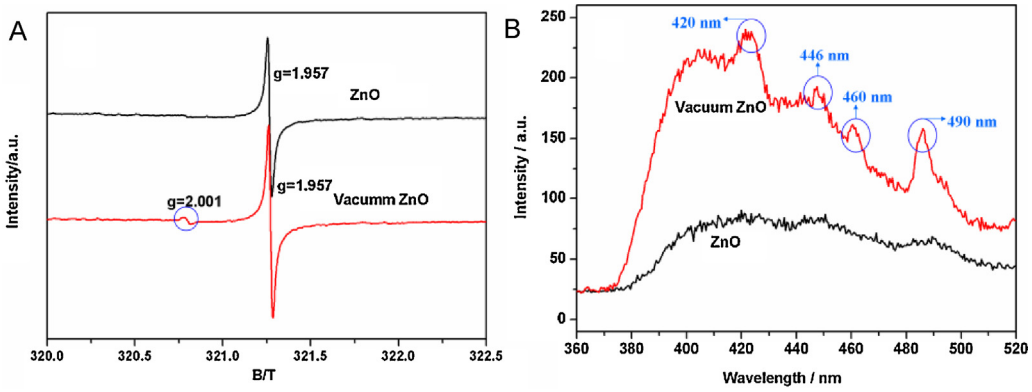

Fig. 4. (A) Situ EPR spectra of ZnO and vacuum ZnO; (B) The PL spectra of ZnO and vacuum ZnO, at wavelength 277 nm excitation.

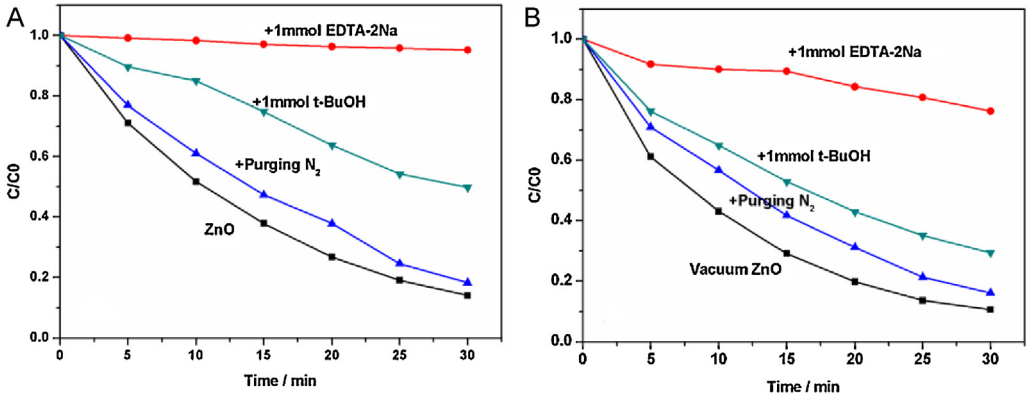

Fig. 5. The plots of photogenerated carriers trapping in the system of photodegradation of MB by (A) ZnO and (B) vacuum ZnO, under UV light, respectively.

3.3. *Mechanism of enhancement of UV activity and generation of visible activity*

It is important to detect main oxidative species in the photocatalytic process for elucidating the photocatalytic mechanism. The main oxidative species in photocatalytic process could be detected through trapping experiments of radicals, holes and $\cdot O_2^-$ by using t-BuOH (radical scavenger)[39] and EDTA-2Na (hole scavenger) [40], and purging N_2 ($\cdot O_2^-$ scavenger) [41], respectively. Under UV light, in ZnO system, the addition of t-BuOH and purging N_2 gas only cause a small change in the photodegradation of MB, as shown in Fig. 5A. On the contrary, the photocatalytic activity of ZnO could be greatly prevented by the addition of a scavenger for holes (EDTA-2Na). The results suggest that the photogenerated holes are the main oxidative species of ZnO system. From Fig. 5B, it can be seen that in vacuum ZnO system, the photocatalytic activity is also greatly suppressed by the EDTA-2Na, the main oxidative species is the same as that of in ZnO system.

As discussed above, particle size (Fig. S1) and the crystal phase structure (Fig. S2) are not evidently changed and the limited adsorptivity enhancement (Fig. S5) is not the major factor of the enhancement of the photocatalytic activity of vacuum ZnO. The significant enhancement of UV photocatalytic activity of vacuum ZnO is mainly due to the high charge separation efficiency induced by surface oxygen-vacancies states. A proposed schematic for electron–hole separation and photocatalytic reaction process of vacuum ZnO photocatalyst is shown in Fig. 6. The VB width can be broadened due to the formation of surface oxygen-vacancies states with energy slightly above and partly overlapping with the VB. This is beneficial to increase the transport rate of photogeneration carriers, resulting in charge separation

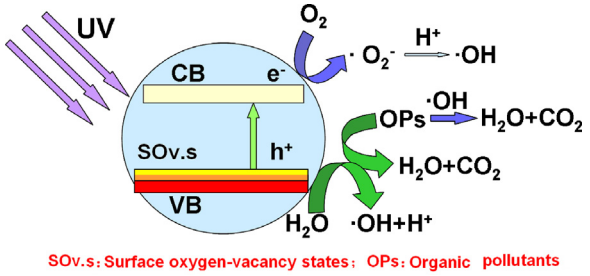

Fig. 6. Schematic drawing illustrates the mechanism of charge separation and photocatalytic reaction process of vacuum ZnO photocatalyst, under UV light.

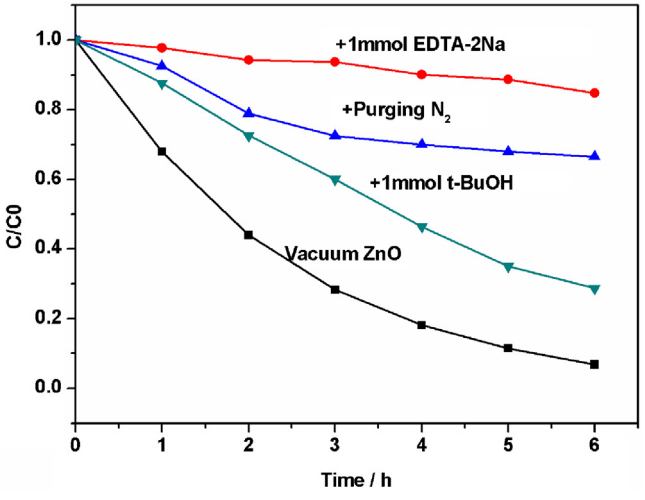

Fig. 7. The plots of photogenerated carriers trapping in the system of photodegradation of MB by vacuum ZnO, under visible light.

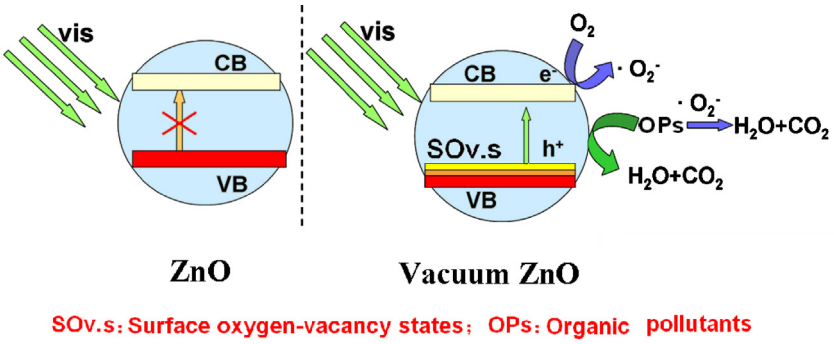

Fig. 8. Schematic drawing illustrates the mechanism of charge separation and photocatalytic reaction process of vacuum ZnO photocatalyst, under visible light.

more efficient and reducing the probability of photogenerated electron–hole recombination, leading to an enhanced photocatalytic activity.

ZnO itself can not be excited by visible light. As a result, the trapping experiment of radicals and holes was only performed on vacuum ZnO photocatalyst under visible light, as shown in Fig. 7. The photodegradation of MB is obviously suppressed after the addition of a scavenger for holes (EDTA-2Na). This indicates that photogenerated hole is the main oxidative species in vacuum ZnO system, which is as same as that of ZnO and vacuum ZnO under UV light. The photocatalytic mechanism of vacuum ZnO under visible light is as same as that of under UV light.

The proposed schematic for the visible activity and photocatalytic reaction process of vaccum ZnO photocatalyst is shown in Fig. 8. The broadening of the VB due to the existence of surface oxygen-vacancies states can decrease the energy band gap. The site of surface oxygen-vacancies states is determines by the concentration of surface oxygen vacancies. When the concentration is too low, the site of surface oxygen-vacancies states will be mostly overlapped with the VB; while the concentration is too high, oxygen vacancies states will be in the forbidden band above the VB. Here bulk oxygen vacancies in ZnO lattice easily generate, which are the recombination center of electron–hole pairs and result in the decrease of photocatalytic activity. The concentration of surface oxygen vacancies can be controlled in an optimum range by tuning vacuum temperature and time. From Fig. 2A, B, it can be found that ZnO after vacuum treated at 255 °C for 5 h shows the highest visible activity. So vacuum ZnO (treated at 255 °C for 5 h) can be successfully excited by visible light, the photogenerated electrons transit to the conduction band (CB), holes would subsequently oxidize organic pollutants absorbed on the surface of vacuum ZnO.

In addition, in ZnO and vacuum ZnO systems, the photogeneration holes are both the main oxidative species, and •OH and O_2^- radicals play an assistant role on the degradation of MB. However, in the process of visible photocatalytic degradation, •O_2^- plays a more important role than •OH radicals, besides the leading role of holes, which is contrary with that of under UV light. This may be because: low-energy visible light merely excites photocatalyst generating fewer holes, and most of holes react with organic pollutants in solution directly, hardly no holes can be react with H_2O transformed to •OH radicals; while high-energy UV light can produce luxuriant holes relatively, many holes still can be transformed to ·OH radicals besides degrading organic pollutants directly, and part of O_2^- radicals also translate to •OH radicals. So the visible photocatalytic activity is greatly reduced after purging N_2 gas into, comparing with the addition of t-BuOH. The conclusion could be drawn that holes are the main oxidative species, and •OH and O_2^- radicals play a role on the degradation of MB in vacuum ZnO system.

4. Conclusions

ZnO photocatalysts with surface oxygen vacancies were prepared via a facile vacuum deoxidation. After vacuum treated, the ZnO photocatalyst possessed significantly enhanced UV light photocatalytic activity and distinct visible light photocatalytic activity. The enhancement of UV activity is attributed to the high separation efficiency of photogenerated electron–hole pairs caused by the broadening of VB width induced by surface oxygen-vacancies states. And the generation of visible activity originates from the narrow of energy band gap due to the rise of valance band maximum. This approach is proposed to develop a new type of optical materials and to be extended for other wide bandgap materials.

Acknowledgements

This work was partly supported by the National Natural Science Foundation of China (20925725, 50972070 and 51102150) and National Basic Research Program of China (2013CB632403) and National High Technology Research and Development Program of China (2012AA062701) and Special Project on Innovative Method from the Ministry of Science and Technology of China (No. 2009IM030500).

Appendix A. Supplementary data

Supplementary data associated with this article can be found, in the online version, at http://dx.doi.org/10.1016/j.apcatb.2013.02.011.

References

[1] M.R. Hoffman, S.T. Martin, W. Choi, D.W. Bahnemann, Chemical Reviews 95 (1995) 69–96.
[2] Y.M. Lin, D.Z. Li, J.H. Hu, G.C. Xiao, J.X. Wang, W.J. Li, X.Z. Fu, Journal of Physical Chemistry C 116 (2012) 5764–5769.
[3] C. Hyeok, J.K. Yong, S.V. Rajender, D.D. Dionysios, Chemistry of Materials 18 (2006) 5377–5384.
[4] X.Z. Fu, A.Z. Walter, M.A. Andreson, Applied Catalysis B 6 (1995) 209–224.
[5] D. Ollis, E. Pelizzetti, N. Serpone, Environmental Science and Technology 25 (1991) 1522–1529.
[6] M.Y. Guo, A.M.C. Ng, F.Z. Liu, A.B. Djurišić, W.K. Chan, H.M. Su, K.S. Wong, Journal of Physical Chemistry C 115 (2011) 11095–11101.
[7] D.W. Chu, Y. Masuda, T. Ohji, K. Kato, Langmuir 26 (2010) 2811–2815.
[8] E.S. Jang, J.H. Won, S.J. Hwang, J.H. Choy, Advanced Materials 18 (2006) 3309–3312.
[9] K. Sato, M. Aoki, R. Noyori, Science 281 (1998) 1646–1647.
[10] V. Subramanian, E. Wolf, P.V. Kamat, Journal of Physical Chemistry B 105 (2001) 11439–11446.
[11] R. Asahi, T. Morikawa, T. Ohwaki, K. Aoki, Y. Taga, Science 13 (2001) 269–271.
[12] J.C. Liu, H.W. Bai, Y.J. Wang, Z.Y. Liu, X.W. Zhang, D.D. Sun, Advanced Functional Materials 20 (2010) 4175–4181.
[13] C.P. Sibu, S.R. Kumar, P. Mukundan, K.G.K. Warrier, Chemistry of Materials 14 (2002) 2876–2881.

[14] S.C. Padmanabhan, S.C. Pillai, J. Colreavy, S. Balakrishnan, D.E. McCormack, T.S. Perova, Y. Gun′ko, S.J. Hinder, J.M. Kellys, Chemistry of Materials 19 (2007) 4474–4481.
[15] R.S. Mane, W.J. Lee, H.M. Pathan, S.H. Han, Journal of Physical Chemistry B 109 (2005) 24254–24259.
[16] A.J. Reddy, M.K. Kokila, H. Nagabhushana, J.L. Rao, C. Shivakumara, B.M. Nagabhushana, R.P. Chakradhar, Spectrochimica Acta, Part A 81 (2011) 59–63.
[17] K. Vanheusden, W.L. Warren, C.H. Seager, D.R. Tallant, J.A. Voigt, B.E. Gnade, Journal of Applied Physics 79 (1996) 9783.
[18] P.H. Kasai, Physical Review 130 (1963) 989–995.
[19] M. Kakazey, M. Vlasova, M. Dominguez-Patino, G. Dominguez Patin o, T. Srec'kovic, N. Nikolic, Science of Sintering 36 (2004) 65–72.
[20] J.C. Conesa, J. Soria, Journal of Physical Chemistry 86 (1982) 1392–1395.
[21] B.K. Meyer, Physica Status Solidi 241 (2004) 231–260.
[22] V. Ischenko, S. Polarz, D. Grote, V. Stavarache, K. Fink, M. Driess, Advanced Functional Materials 15 (2005) 1945–1954.
[23] I. Nakamura, N. Negishi, S. Kutsuna, T. Ihara, S. Sugihara, K. Takeuchi, Journal of Molecular Catalysis A: Chemical 161 (2000) 205–212.
[24] C.P. Kumar, N.O. Gopal, T.C. Wang, M.S. Wong, S.C. Ke, Journal of Physical Chemistry B 110 (2006) 5223–5229.
[25] D.C. Cronemeyer, Physical Review 113 (1959) 1222–1226.
[26] L.W. Zhang, L. Wang, Y.F. Zhu, Advanced Functional Materials 17 (2007) 3781–3790.
[27] Z.S. Lin, A. Orlov, R.M. Lambert, M.C. Payne, Journal of Physical Chemistry B 109 (2005) 20948–20952.
[28] X.L. Xu, S.P. Lau, J.S. Chen, G.Y. Chen, B.K. Tay, Journal of Crystal Growth 223 (2001) 201–205.
[29] S. Mahamuni, K. Borgonhain, B.S. Bender, V.J. Leppert, S.H. Risbud, Journal of Applied Physics 85 (1999) 2861–2865.
[30] Z.Y. Xue, D.H. Zhang, Q.P. Wang, J.H. Wang, Applied Surface Science 195 (2002) 126–129.
[31] K.W. Wong, M.R. Field, J.Z. Ou, K. Latham, M.J. Spencer, I. Yarovsky, K. Kalantar-zadeh, Nanotechnology 23 (2012), 015705.
[32] C.F. Windisch, G.J. Exarhos, C.H. Yao, L.Q. Wang, Journal of Applied Physics 101 (2007) 123711–123717.
[33] M. Scepanovic, B.M. Grujic, K. Vojisavljevic, S. Bernik, T. Sreckovic, Journal of Raman Spectroscopy 41 (2009) 914–921.
[34] E.G. Bylander, Journal of Applied Physics 49 (1978) 1188.
[35] F.A. Kröoger, H.J. Vink, Journal of Chemical Physics 22 (1954) 250–252.
[36] S.J. Pearton, D.P. Norton, K. Ip, Y.W. Heo, T. Steiner, Progress in Materials Science 50 (2005) 293–340.
[37] L.Q. Jing, Y.C. Qu, B.Q. Wang, S.D. Li, B.J. Jiang, L.B. Yang, W. Fu, H.G. Fu, J.Z. Sun, Solar Energy Materials and Solar Cells 90 (2006) 1773–1787.
[38] L.Q. Jing, F.L. Yuan, H.G. Hou, B.F. Xin, W.M. Cai, H.G. Fu, Science in China Series B: Chemistry 48 (2005) 25–30.
[39] H. Lee, W. Choi, Environmental Science and Technology 36 (2002) 3872–3878.
[40] J. Zhou, C. Deng, S. Si, Y. Shi, X. Zhao, Electrochimica Acta 56 (2011) 2062–2067.
[41] C.S. Pan, Y.F. Zhu, Environmental Science and Technology 44 (2010) 5570–5574.